High-Temperature Oxidation Behavior of Ti6242S Ti-based Alloy

Aurélie Vande Put, Charlotte Dupressoire, Carole Thouron, Philippe Emile, Raphaëlle Peraldi, Benjamin Dod, Daniel Monceau

https://doi.org/10.1007/s11085-021-10073-4

High-Temperature Oxidation Behavior of Ti6242S Ti-based Alloy

Aurélie Vande Put[1] · Charlotte Dupressoire[1,2] · Carole Thouron[1] · Philippe Emile[2] · Raphaëlle Peraldi[2] · Benjamin Dod[2] · Daniel Monceau[1]

Abstract
The aircraft industry is always looking for improved efficiency through higher in-service engine temperatures and lighter structures. Titanium-based alloys are good candidates for such applications because of their high specific strength. However, when exposed to high-temperature oxidizing environments, a large amount of dissolved oxygen can be found in such alloys beneath the growing oxide scale, possibly leading to embrittlement. Consequently, evaluating the oxidation resistance of these alloys is essential. With this aim, long-term oxidation tests were carried out on Ti6242S alloy between 500 and 650 °C to study the effect of temperature, surface preparation and microstructure on oxide scale and oxygen dissolution. While increasing the temperature from 560 to 625 °C led to accelerated oxidation kinetics, surface preparation had no noticeable effect on mass variations and oxygen diffusion profiles. Regarding microstructure, when comparing Ti6242S samples having similar α-phase fraction but very different microstructures (fineness and morphology), there wasn't any significant effect found on mass change and oxygen diffusion after 1 kh at 650 °C.

Keywords High-temperature oxidation · Titanium-based alloy · Oxygen dissolution

Introduction

As economic and environmental requirements become increasingly strict, the aeronautic industry is determined to lighten aircrafts by introducing more Ti-based alloys because of their high specific mechanical properties and their good compatibility with carbon fiber-reinforced polymers. However, under operating conditions, some

✉ Aurélie Vande Put
aurelie.vandeput@ensiacet.fr

parts made of Ti-based alloys are exposed to high temperatures (up to 650 °C) and important oxidation phenomena can appear. The oxidation of these alloys involves the formation of a TiO_2 oxide scale and the dissolution of large amounts of oxygen within the material. For instance, pure titanium can dissolve up to 33 at.% and 8 at.% oxygen in α and β phases, respectively, at high temperatures [1]. This oxygen diffusion can greatly affect the ductility [2–5], and therefore the durability of Ti-based alloys, limiting the maximum temperature at which they can be used in long-term applications. The present study focuses on the influence of surface preparation and microstructure on the oxidation behavior of Ti6242S.

Champin et al. studied the oxidation behavior for 80 days at 550 and 600 °C of 685 alloy (Ti–6Al–5Zr–0.5Mo–0.25Si) exhibiting three surface states: rolled, grit blasted and ground using P600 SiC paper. They observed that reducing surface roughness led to a decrease in mass gain [6]. In the specific case of additively manufactured alloys, the large surface area resulting from this fabrication process leads to faster oxidation kinetics. This large surface area can be reduced through grinding, as shown by Casadebaigt et al. who oxidized TA6V (Ti–6Al–4V) alloys obtained by laser and electron beam melting in the 500–600 °C temperature range [7]. Shot-peening was also used by various researchers to improve the properties of commercially pure Ti [8–10] and Ti-based alloys [11, 12]. After oxidation for only 1 h at 700 °C, Wen et al. noticed a slight increase in O, N and C contents in the near surface of commercially pure Ti after shot-peening followed by light grinding (aimed at removing 3–6 μm) [8]. After a much longer time (1800 h) at the same temperature in laboratory air, Thomas et al. noticed a large increase in O quantity under the surface of an IMI834 alloy (Ti–5.8Al–4Sn–3.5Zr–0.7Nb–0.5Mo–0.35Si–0.06C) subjected to shot-peening before oxidation [11]. Authors attributed this increase in O diffusion to the introduction of mechanical twins and pointed out that O diffusion was accompanied by silicide precipitation along the mechanical twin boundaries and in areas with high dislocation density. On the other hand, other researchers reported a decrease in mass variation of shot-peened samples oxidized at 700 °C, due to the formation of a N-rich layer at the oxide/alloy interface [9]. However, the operating temperatures of Ti-based alloys rarely, if ever, reach 700 °C, even for alloys designed for the highest operating temperatures, such as Ti6242S (Ti–6Al–2Sn–4Zr–2Mo–Si), which is known to exhibit a good oxidation resistance [5, 13–15] and is the material of this study. Excessively high temperatures can modify oxidation regimes, as shown in Ti6242 and Ti6242S alloys by Calvert and Kosaka and Gaddam et al., respectively [13, 15]. This can also lead to modified contents of alloying elements between phases, as found in the TA6V alloy [16, 17].

Regarding microstructure, many works reported its influence on the oxidation behavior of Ti-based alloys [13, 18–21]. Many researchers consider that grain boundaries and interphases favor oxygen diffusion [13, 18, 20]. Rosa determined that oxygen diffuses faster in the β phase than in the α phase [22]. Based on their work on IMI834 alloy, Sai Srinadh et al. reported that, after being oxidized at 750 and 800 °C in laboratory air, a duplex microstructure leads to higher mass variations than a lamellar one [18]. Nevertheless, they obtained very similar mass changes for oxidations at 600 °C and 650 °C. At 760 °C, Pitt et al. did not notice a significant difference in mass changes after the oxidation of two globular TA6V with

two different grain sizes [20]. These authors claim that the different grain sizes of their alloys greatly affected the oxygen ingress in the metal. Nevertheless, the hardness profiles they obtained were similar apart from an offset. The hardness profiles evidently show that both alloys had similar oxygen diffusion coefficients. Then, the offset could be due to the fact that the two studied alloys (small and large grains) had different nominal levels of oxygen (0.16 and 0.08 wt.%, respectively), or because of the way the hardness was normalized. This leads to the conclusion that grain size has little or no effect on oxygen diffusion. The same conclusions were drawn by Casadebaigt et al. on a TA6V alloy made by additive manufacturing [17]. For these alloys manufactured using electron and laser beam melting, authors reported that a hot isostatic pressure (HIP) treatment did not have an effect on mass variations nor on oxygen diffusion coefficients, despite an important coarsening of the microstructure resulting from the HIP. Finally, Sugahara et al. oxidized TA6V samples exhibiting a globular microstructure on the one hand and a Widmanstätten microstructure on the other for 48 h between 500 and 600 °C. They reported similar mass changes for both sets of samples even though their grain sizes were very different [23].

These studies on the influence of surface and microstructure were often conducted at temperatures that are higher and for durations that are shorter than those found in real applications. Long-term oxidations carried out at lower temperatures are necessary in order to investigate the effect of surface preparation and microstructure that are closer to industrial applications. A microstructure comparison should also be performed on materials with similar volume fractions of α and β phases, to study the influence of microstructure morphology on oxygen diffusion. In this work, Ti6242S Ti-based alloy was oxidized between 500 and 650 °C for durations of up to 10 kh. Both the oxide scale and the oxygen dissolution were characterized by X-ray diffraction (XRD), Raman and fluorescence spectroscopies, scanning electron microscopy (SEM) and Vickers microhardness to determine the influence of these two parameters on the oxidation behavior.

Experimental Procedures

Materials

Two Ti6242S alloys supplied by Aubert &Duval (Pamiers, France) were used in the present work. To study the effect of surface preparation, oxidation tests

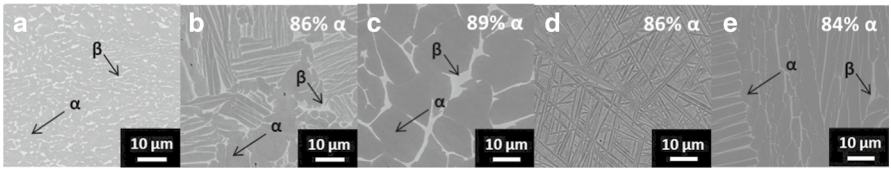

Fig. 1 Ti6242S alloy microstructures (SEM images, BSE mode): **a** hot rolled Ti6242S, **b–e** forged Ti6242S: **b** duplex, **c** globular, **d** fine lamellar, **e** coarse lamellar

Table 1 Composition of Ti6242S alloys (*ppm)

Element	Ti	Al	Sn	Zr	Mo	Si	O*	N*	C*	S*	H*
Rolled											
wt.%	Bal	6.3	2.0	3.7	1.6	750*	850	13	19	< 5	30
at.%	Bal	11.0	0.8	1.9	0.8	0.1	2500	44	75	< 7	1400
Forged											
wt.%	Bal	6.0	1.8	4.0	2.1	0.1	1200	< 5	26	8.2	44
at.%	Bal	10.5	0.7	2.1	1.0	0.2	3550	< 17	103	12	2062

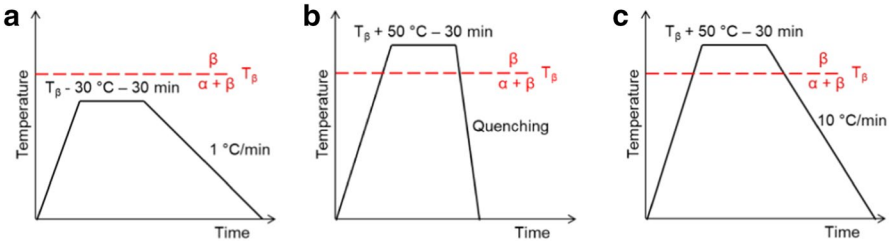

Fig. 2 Heat treatments applied for additional microstructures: **a** globular, **b** fine lamellar, **c** coarse lamellar

were carried out on a Ti6242S alloy exhibiting an α/β globular microstructure (Fig. 1a) resulting from a hot rolling below β transus followed by a duplex annealing, as per AMS4919 (899 °C/30 min air cooling + 788 °C/15 min air cooling). The effect of microstructure was studied using a forged Ti6242S that underwent a solution heat treatment of 1h45 at 985 °C followed by a blast air cooling and an aging at 593 °C for 9 h, leading to a duplex microstructure (Fig. 1b). Composition was measured by energy-dispersive X-ray spectroscopy (EDS) at the CIRIMAT laboratory and instrumental gas analysis (IGA) by Evans Analytical Group SAS (EAG, Tournefeuille, France) for heavy elements and light elements, respectively. Glow discharge mass spectrometry (GDMS) was also realized by EAG SAS on the rolled Ti6242S alloy, to determine its Si content. Compositions are given in Table 1, and microstructures are shown in Fig. 1.

To study microstructure, three heat treatments were performed on a forged Ti6242S alloy to obtain additional microstructures such as globular, fine and coarse lamellar. Blocks of $15 \times 15 \times 40$ mm^3 were cut from the initial block and treated. Samples were machined from these blocks as thin plates of approximately $12 \times 12 \times 2$ mm^3, whereas those from the initial microstructure measured $20 \times 20 \times 2$ mm^3. Details on heat treatments and obtained microstructures are shown in Figs. 1c–e and 2, respectively. α-phase fractions were determined by image analysis using Aphelion 4.3.1 software, with an accuracy of 5%. About ten

images with a representative surface of the microstructure were used (0.30 mm^2 and 0.0081 mm^2 for the globular and lamellar microstructures, respectively).

Oxidation tests

The effect of surface preparation on long-term oxidation was studied using parallelepipedic specimens ($19.7 \times 19.7 \times 3.97$ mm^3) positioned on ceramic bricks in Nabertherm N60/85HA and N120/85HA furnaces. The majority of the specimens were ground using P240 SiC paper. Others received no surface preparation, and a few were either cut from plates after super plastic forming (SPF) or ground using P80 SiC paper or mirror polished (using 0.5 μm Al_2O_3 particles). Oxidation tests were performed under circulating laboratory air for up to 10 kh at 500 and 560 °C, and for up to 997 h at 625 °C, with a few intermediate removals to monitor specimen mass changes. A Mettler Toledo XP56, with a mass resolution of 0.1 μg, was used for mass measurements before, during and after oxidation. Each recorded mass change was the average of two weighings.

The microstructure influence was analyzed on parallelepipedic ($15 \times 10 \times 1$ mm^3) specimens ground using P240 SiC paper. The oxidation test ran at 650 °C for 1 kh in flowing synthetic air + 5% H_2O with a flux of 95 mL min^{-1}. Weighings were performed before, during and after oxidation, three times per specimens, with a Sartorius Genius (ME215-P) balance, with an accuracy of 20 μg.

Characterization

To characterize oxide scale phases, XRD was performed using a copper anti-cathode ($\lambda = 1.54056$ Å). XRD analyses were done using a BRUKER D8-2 and a 3000TT-Seiffert apparatus with a low incidence of 2° to 8°, a Bragg angle between 20° and 80° (in 2θ), with a step of 0.04 or 0.05° and an acquisition time of 6 to 10 s per step. To further complete oxide identification, a Labram HR 800 spectrometer from Horiba Yvon Jobin, equipped with a confocal microscope, was used for Raman and fluorescence spectroscopy with a laser characterized by a 532 nm wavelength. Raman spectroscopy was performed to detect anatase and rutile TiO_2, while the presence of alumina and its allotropic forms was identified by fluorescence spectroscopy. Observations of sample surfaces and cross sections after heat treatments and oxidations were performed by SEM with a LEO435VP microscope using the backscattered electron (BSE) mode. Oxygen enrichment in the material was characterized by Vickers microhardness profiles obtained with a Buehler OmniMet 2100 Series microhardness tester and using a 50 g diamond indent.

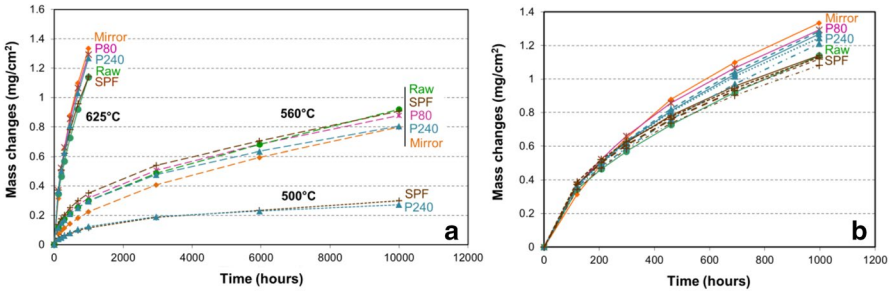

Fig. 3 Mass changes during long-term oxidations in circulating laboratory air of hot rolled Ti6242S alloy **a** for one sample per surface preparation and temperature and **b** for all tested specimens at 625 °C (including duplicate specimens with a SPF and P240 ground surface state)

Results and Discussion

Effect of Surface Preparation

Mass variations measured during and after oxidation for up to 10 kh at 500 °C and 560 °C and up to 997 h at 625 °C on rolled Ti6242S exhibiting various surface preparations are reported in Fig. 3. Oxidation kinetics were parabolic. No particular trend can be deduced from these data concerning the effect of surface preparation. Very similar mass variations were measured after 10 kh at 500 °C for a ground surface and a SPF surface state. Among the five surface preparations tested at 560 °C and 625 °C, small differences in mass variations were noticed after 10 kh and 997 h, respectively. However, they are not significant and the ranking observed between surface states is not the same for both temperatures. Finally, duplicate specimens with a SPF surface state or ground with P240 SiC paper were oxidized at 625 °C (Fig. 3b). Close mass variations were obtained for a given surface preparation, highlighting the good reproducibility of the results.

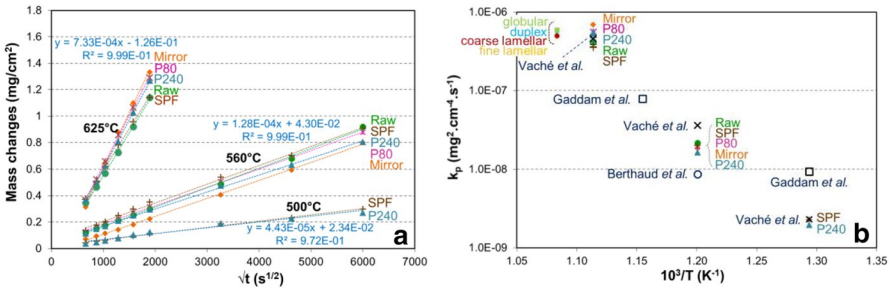

Fig. 4 **a** Mass changes during long-term oxidations under circulating laboratory air of hot rolled Ti6242S alloy and equations of the linear laws applied to the samples ground with P240 SiC paper for k_p determination; **b** Arrhenius plot of the parabolic oxidation constants of Ti6242S alloy oxidized at 500, 560, 625 and 650 °C and comparison with data from the literature (Gaddam et al. [15], Berthaud et al. [14], Vaché et al. [24])

Parabolic oxidation constants, k_p, were calculated using Eq. 1, based on mass variations from 100 h to 997 or 10 kh, i.e., after the transient stage:

$$\frac{\Delta m}{S} = \sqrt{k_p \times t} + C \quad (1)$$

with $\frac{\Delta m}{S}$ the mass variation, t the time and C a constant.

Figure 4a displays the equations corresponding to a linear law applied to the mass variation versus the square root of oxidation time, for samples ground using P240 SiC paper. These equations, used to determine the parabolic oxidation constants, reveal that the C constant of Eq. 1 is negligible in the present study, i.e., for long oxidation exposures. Parabolic oxidation constants at 500 °C are equal to 2.0×10^{-9} and 2.3×10^{-9} mg^2 cm^{-4} s^{-1} for P240 and SPF surfaces, respectively. This is in fair agreement with the study of Gaddam et al. who estimated a parabolic constant value of 9.34×10^{-9} mg^2 cm^{-4} s^{-1} for Ti6242S oxidized at 500 °C in ambient air but for a much shorter time (500 h) [15]. Parabolic oxidation constants range from 1.7×10^{-8} to 2.1×10^{-8} mg^2 cm^{-4} s^{-1} at 560 °C, while they range from 3.6×10^{-7} to 6.9×10^{-7} mg^2 cm^{-4} s^{-1} at 625 °C. Both intervals surround the parabolic oxidation constant determined by Gaddam et al. for Ti6242S oxidized at 593 °C for 500 h (namely 7.84×10^{-8} mg^2 cm^{-4} s^{-1}) [15]. Finally, k_p values obtained at 560 °C are higher but close to the one determined by Berthaud et al. on a Ti6242S oxidized 10 kh at 560 °C (namely 8.7×10^{-9} mg^2 cm^{-4} s^{-1}) after a grinding using P600 SiC paper [14]. At 500, 560 and 625 °C, the recent review from Vaché et al. gave parabolic constant values of 2.3×10^{-9}, 3.6×10^{-8} and 4.6×10^{-7} mg^2 cm^{-4} s^{-1}, respectively, from a database that includes varying surface states [24]. These values are also in good agreement with those found in the present study. All these data are placed on an Arrhenius plot in Fig. 4b for an easier comparison.

XRD analyses, Raman and fluorescence spectroscopies as well as SEM observations were performed on ground samples (P240 SiC paper) after oxidation at 500, 560 and 625 °C. While anatase TiO_2 and rutile TiO_2 were present at each temperature, α-alumina was only detected at 560 °C and 625 °C. Oxide scales formed during oxidation at 560 °C and 625 °C are shown in Fig. 5. The mass variations and the oxide scale thickness are much higher after 997 h at 625 °C than after 10 kh at 560 °C. From 560 °C, a 65-degree increase led to a significant increase in the oxidation kinetics of the rolled Ti6242S alloy. Taking into account a mean parabolic oxidation constant equal to 2.65×10^{-8} mg^2 cm^{-4} s^{-1} and 7.45×10^{-7} mg^2 cm^{-4} s^{-1} at 560 °C and 625 °C, respectively, the oxidation kinetics was multiplied by a factor 28 due to the 65 °C temperature increase.

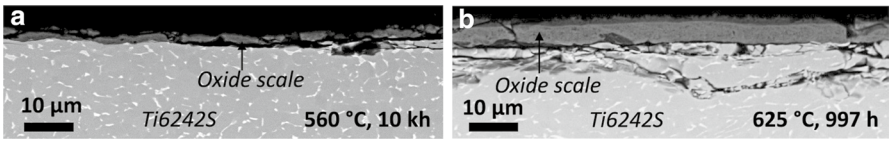

Fig. 5 SEM images (BSE mode) of cross sections of hot rolled Ti6242S, ground using P240 SiC paper, after an oxidation in circulating laboratory air **a** for 10 kh at 560 °C and **b** for 997 h at 625 °C

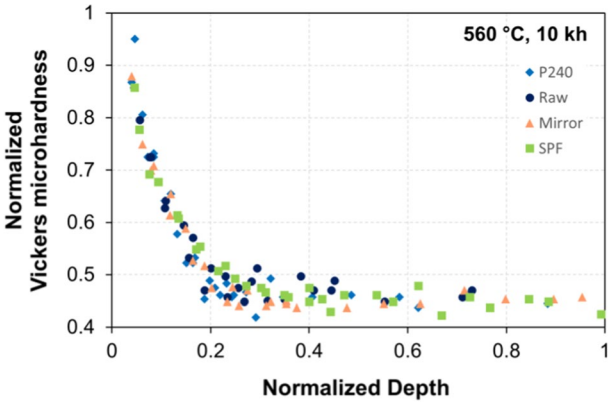

Fig. 6 Normalized Vickers microhardness profiles on rolled Ti6242S alloys with different surface preparations and oxidized in circulating laboratory air for 10 kh at 560 °C

Regarding the microstructure of the alloy, there is no noticeable difference between the two samples. However, after being oxidized at 625 °C, Ti6242S exhibits many cracks underneath the oxide/alloy interface (Fig. 5b). This embrittlement could come from the metallographic preparation and/or from a larger oxygen diffusion during oxidation. To further characterize this, microhardness measurements were made on various specimens, from the oxide/alloy interface toward the bulk. Figure 6 reports the normalized Vickers microhardness profiles of Ti6242S after different surface preparations and an oxidation at 560 °C for 10 kh. (Data were normalized because of confidentiality.) These profiles do not reveal any major difference. It can be reminded that among the samples oxidized at 560 °C, only small mass variation differences were found. Therefore, it seems fair to conclude that, between 500 °C and 625 °C, surface preparation has little effect on the long-term oxidation of a rolled Ti6242S alloy.

Effect of Initial Microstructure

Because oxygen solubility in α-Ti and β-Ti is very different, the effect of alloy microstructure on the oxidation behavior was studied with similar volume fractions of α-Ti phase. This was done in order to focus on the influence of microstructure morphology. In this work, α-phase proportion was the same in the four microstructures (between 84 and 89% with a measurement accuracy of 5%). The effect of initial microstructure on oxidation kinetics at 650 °C for 1 kh is shown in Fig. 7. Mass changes follow the same trend in all microstructures studied here. From Eq. 1 and based on the mass variations between 100 and 1000 h, parabolic oxidation constants were found equal to 5.3×10^{-7}, 5.9×10^{-7}, 4.9×10^{-7} and 5.0×10^{-7} $mg^2\ cm^{-4}\ s^{-1}$ for the duplex, globular, fine lamellar and coarse lamellar microstructures, respectively. These values show that, at 650 °C, microstructure morphology (Fig. 1) does not have a significant effect on mass variation.

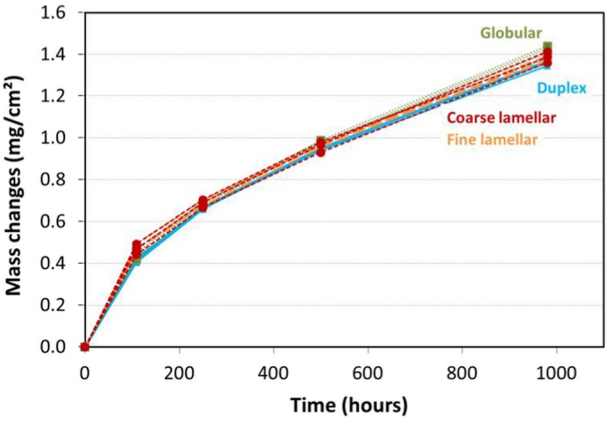

Fig. 7 Mass changes of forged Ti6242S microstructures after 1 kh at 650 °C under flowing synthetic air + 5% H_2O

The oxidation kinetics at 650 °C are similar to those previously obtained at 625 °C when studying the influence of surface preparation (Fig. 4b). For a given oxidation temperature under different oxidizing atmospheres (ambient air, synthetic air, circulating laboratory air), Casadebaigt et al. noticed a discrepancy among the various oxidation kinetics values found in the literature for TA6V alloy [7]. In the present study, the tests at the highest temperature (650 °C) were performed under a low velocity synthetic air + 5 vol% H_2O flow whereas the tests performed at lower temperatures (including 625 °C) were carried out in a circulating laboratory air flow. The fact that the gas velocity applied to samples tested under synthetic air + 5 vol% H_2O was low could have limited the oxidation kinetics at 650 °C. This could explain the similar mass gains found at 650 °C and 625 °C. Another explanation could be the fact that the composition of Ti6242S varies between the two series of experiments (Table 1). Indeed, the nominal oxygen content is much higher in the forged alloy than in the rolled one. Using a 1D finite differences numerical model, Ciszak et al. studied Ti-based alloys and the influence of nominal oxygen content on their life span under oxidizing conditions [25]. Considering that the oxygen-affected zone (OAZ) corresponds to the metal thickness with an oxygen content superior or equal to 0.5 at.%, and that the component reaches its life span when the OAZ thickness amounts to about 10% of its overall thickness, they found that an increase in nominal oxygen content is associated with a decrease in life span. This means that the higher the nominal oxygen content, the less dissolved oxygen quantity is needed to reach the oxygen solubility limit of the alloy. It should be reminded that the oxygen content in the forged Ti6242S alloy oxidized at 650 °C is higher than that of the rolled Ti6242S alloy tested at 650 °C. Assuming that the oxygen solubility limit does not vary significantly if the temperature is changed from 625 to 650 °C, the greater oxygen content of the forged alloy should result in a lesser quantity of diffused oxygen within the alloy during the oxidation at 650 °C. This may be a second reason that could explain the similar oxidation kinetics found in both experiments.

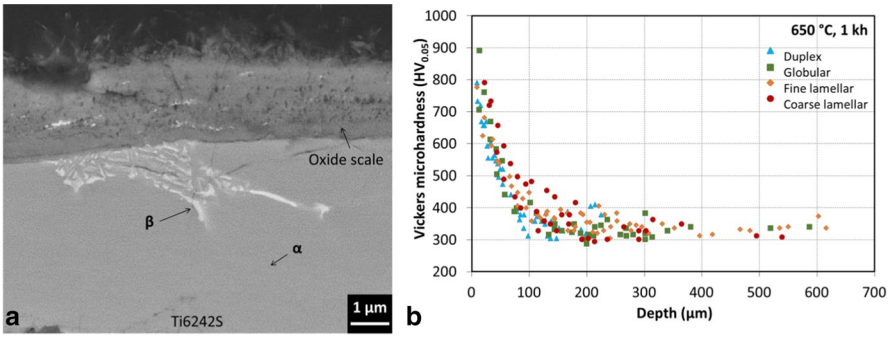

Fig. 8 After an oxidation of 1 kh at 650 °C under flowing synthetic air + 5% H_2O: **a** SEM image (BSE mode) of a cross section of the forged and duplex Ti6242S sample, **b** Vickers microhardness profiles obtained in the forged Ti6242S samples with various microstructures

Figure 8a shows a cross section of the oxide scale present on the alloy with a duplex microstructure. Observations revealed a porous inner layer of 2.1 µm with needles above it. XRD analyses, associated with Raman and fluorescence spectroscopies, indicated that the oxide scale was composed of anatase, rutile and α-alumina. It was also noticed that the metal was brittle, as cracks were visible directly under the oxide/alloy interface. These cracks could have emerged from the metallographic preparation because of the alloy embrittlement due to oxygen dissolution. Microhardness profiles are shown in Fig. 8b to characterize the oxygen diffusion inside the microstructures. Despite a certain variation in Vickers microhardness for a given profile, it is reasonable to say that, near the surface, Vickers microhardness is the same for all microstructures. Affected depths were also similar after 1 kh at 650 °C.

These results are in contradiction with the study by Satko et al. who also produced their microstructures from the same thick sheets of mill-annealed Ti6242S alloy [21]. After an oxidation of 420 h at 650 °C, they noticed a gap of about 0.25 mg cm^{-2} between the mass variations of the five microstructures while the dispersion difference was only of about 0.1 mg cm^{-2} between the mass variations obtained in the present study after 1000 h at 650 °C. While efforts were made in the present work to produce microstructures exhibiting similar α-phase contents, Satko et al. oxidized microstructures with different α-phase contents. This could explain the difference between the two studies regarding the influence of microstructure.

From the present results, it can therefore be concluded that for samples with similar α-phase contents and oxidized for up to 1 kh at 650 °C, the microstructure morphology, with varying grain shapes and interface densities, does not have an influence on mass variation nor on oxygen diffusion in Ti6242S. Because a lower temperature should favor diffusion at the interfaces over intragranular diffusion, a similar experiment should be conducted at 500 °C to confirm or infirm this conclusion. This would, however, require a very long experiment.

In addition to bringing interesting results on the effect of surface preparation and microstructure on the oxidation of Ti6242S, these data are important for lifetime predictions. Oxidation kinetics data corresponding to the temperature range studied here and for such exposure durations are rare. In future works, these data could be used to predict lifetimes, as was done by Vaché et al. on Ti64 and Ti6242S Ti-based alloys [24].

Conclusions

Long-term oxidations were carried out between 500 and 650 °C on two Ti6242S alloys, one rolled and one forged, for durations of up to 10 kh. Oxide scales were characterized by XRD, Raman and fluorescence spectroscopies and SEM, while oxygen diffusion within the alloy was studied with Vickers microhardness profiles.

Based on the results obtained after oxidations for 10 kh at 500 and 560 °C and for 997 h at 625 °C on rolled Ti6242S with various surface preparations, and based on the oxidation results for forged Ti6242S with different microstructures, the following conclusions can be drawn. First, the surface preparation had little or no effect on the long-term oxidation behavior in the 500–625 °C temperature interval. Second, samples exhibiting very different microstructures but similar α-phase fractions did not show any significant difference in terms of mass variation and hardness profile after 1 kh at 650 °C.

Acknowledgements This study on the effect of microstructure was supported by the French National Research Agency through the project ANR DUSTI in partnership with Airbus, Airbus Group Innovations, Aubert&Duval, Liebherr Toulouse Aerospace, the Institut Pprime, the Institut Jean Lamour and the CIRIMAT Laboratory. The contributions of Moukrane Dehmas through fruitful discussions are gratefully acknowledged.

References

1. J. L. Murray and H. A. Wriedt, *Bulletin of Alloy Phase Diagrams* **8**, 148–165 (1987).
2. W. L. Finlay and J. A. Snyder, *Journal of Metals* **188**, 227–286 (1950).
3. H. Fukai, et al., *Isij International* **45**, 133–141 (2005).
4. A. Casadebaigt, D. Monceau, and J. Hugues, *MATEC Web of Conferences, The 14th World Conference on Titanium (Ti 2019)*, Vol. 321, 03006 (2020).
5. A. Vande Put et al., *MATEC Web of Conferences, The 14th World Conference on Titanium (Ti 2019)*, Vol. 321, 04011 (2020).
6. B. Champin, et al., *Journal of the Less Common Metals* **69**, 163–183 (1980).
7. A. Casadebaigt, J. Hugues, and D. Monceau, *Oxidation of Metals* **90**, 633–648 (2018).
8. M. Wen, et al., *Colloids and Surfaces B-Biointerfaces* **116**, 658–665 (2014).
9. A. Kanjer, et al., *Oxidation of Metals* **88**, 383–395 (2017).
10. A. Kanjer, et al., *Surface and Coatings Technology* **343**, 93–100 (2018).
11. M. Thomas, et al., *Acta Materialia* **60**, 5040–5048 (2012).
12. L. Lavisse et al., *Surface & Coatings Technology* **403**, 126368 (2020).
13. K. Calvert and Y. Kosaka, Evaluation of titanium alloys after high temperature air exposure, *Proceedings of 13th World Conference on Titanium*, pp. 1605–1612 (2016).
14. M. Berthaud, et al., *Corrosion Science* **164**, 108049 (2020).
15. R. Gaddam, et al., *Materials Characterization* **99**, 166–174 (2015).
16. J. W. Elmer, et al., *Materials Science and Engineering: A* **391**, 104–113 (2005).
17. A. Casadebaigt, J. Hugues, and D. Monceau, *Corrosion Science* **175**, 108875 (2020).

18. K. V. Sai Srinadh and V. Singh, *Bulletin of Materials Science* **27**, 347–354 (2004).
19. C. Leyens, et al., *Materials Science and Technology* **12**, 213–218 (1996).
20. F. Pitt and M. Ramulu, *Journal of Materials Engineering and Performance* **13**, 727–734 (2004).
21. D. P. Satko, et al., *Acta Materialia* **107**, 377–389 (2016).
22. C. J. Rosa, *Metallurgical Transactions* **1**, 2517–2522 (1970).
23. T. Sugahara et al., The Effect of Widmanstatten and Equiaxed Microstructures of Ti-6Al-4V on the Oxidation Rate and Creep Behavior, *Materials Science Forum*, Vol. 636-637, pp. 657–662 (2010).
24. N. Vaché, et al., *Corrosion Science* **178**, 109041 (2021).
25. C. Ciszak, et al., *Corrosion Science* **176**, 109005 (2020).

Authors and Affiliations

Aurélie Vande Put[1] · Charlotte Dupressoire[1,2] · Carole Thouron[1] · Philippe Emile[2] · Raphaëlle Peraldi[2] · Benjamin Dod[2] · Daniel Monceau[1]

Charlotte Dupressoire
charlotte.dupressoire@gmail.com

Carole Thouron
carole.thouron@ensiacet.fr

Philippe Emile
philippe.emile@airbus.com

Raphaëlle Peraldi
raphaelle.peraldi@airbus.com

Benjamin Dod
benjamin.b.dod@airbus.com

Daniel Monceau
daniel.monceau@toulouse-inp.fr

CIRIMAT, Université de Toulouse, CNRS, INP-ENSIACET, 4 allée Emile Monso, BP44362, 31030 Toulouse Cedex 4, France

2 Airbus Operations S.A.S., 316 route de Bayonne, 31060 Toulouse, France